Non-Gaussian Mechanical Motion via Single and Multiphonon Subtraction from a Thermal State

G. Enzian [1,2,3] L. Freisem [1,2] J. J. Price [1,2] A. Ø. Svela [1,2,4] J. Clarke [1] B. Shajilal,[5] J. Janousek [5]
B. C. Buchler,[5] P. K. Lam [5] and M. R. Vanner [1,2,*]

[1]*QOLS, Blackett Laboratory, Imperial College London, London SW7 2BW, United Kingdom*
[2]*Clarendon Laboratory, Department of Physics, University of Oxford, Oxford OX1 3PU, United Kingdom*
[3]*Niels Bohr Institute, University of Copenhagen, Copenhagen 2100, Denmark*
[4]*Max Planck Institute for the Science of Light, Staudtstaße 2, 91058 Erlangen, Germany*
[5]*Centre for Quantum Computation and Communication Technology, Research School of Physics and Engineering,
Australian National University, Canberra 2601, Australia*

Quantum optical measurement techniques offer a rich avenue for quantum control of mechanical oscillators via cavity optomechanics. In particular, a powerful yet little explored combination utilizes optical measurements to perform heralded non-Gaussian mechanical state preparation followed by tomography to determine the mechanical phase-space distribution. Here, we experimentally perform heralded single-phonon and multiphonon subtraction via photon counting to a laser-cooled mechanical thermal state with a Brillouin optomechanical system at room temperature and use optical heterodyne detection to measure the s-parametrized Wigner distribution of the non-Gaussian mechanical states generated. The techniques developed here advance the state of the art for optics-based tomography of mechanical states and will be useful for a broad range of applied and fundamental studies that utilize mechanical quantum-state engineering and tomography.

Introduction.—A key current goal in cavity quantum optomechanics is to generate and fully characterize non-Gaussian states of mechanical motion that exhibit nonclassical behavior. Pursuing this line of research will facilitate the development of mechanical-oscillator-based quantum technology such as quantum memories exploiting the long coherence times available [1–3], coherent transducers [4,5], and sensors [6–8]. Additionally, such state generation and characterization capabilities will help explore fundamental physics including the quantum-to-classical transition [9–11] and even the interface between quantum mechanics and gravity [12–14].

Throughout quantum optics, non-Gaussian state preparation of a bosonic mode followed by phase-space characterization has been performed with a wide spectrum of different platforms. For trapped ions, a single-phonon Fock state of motion of was prepared and reconstructed [15], and multicomponent superposition states are now being studied [16]. In optics, heralded single-photon addition or subtraction followed by homodyne tomography has been widely utilized, with prominent examples including Wigner tomography of a heralded single-photon state [17], single-photon and multiphoton subtraction to squeezed states to generate superposition states [18–20], and photon addition and subtraction to optical thermal states [21–23]. Other notable examples of non-Gaussian quantum states with other physical systems include studying the

decoherence of a superposition state of a microwave field inside a cavity [24], generating non-Gaussian states of atomic-spin ensembles [25], creating arbitrary quantum states in a microwave superconducting circuit [26], and creating nonclassical states of acoustic waves coupled to superconducting qubits [27,28].

Within optomechanics excellent progress utilizing single-photon detection has been made including generating nonclassical states of high-frequency vibrations in diamond crystals [29–31] and photonic-crystal structures [32], second-order-coherence measurements of mechanical modes [33,34], the generation of mechanical interference fringes [35], and single-phonon addition or subtraction to a thermal state resulting in a doubling of the mean occupation [36]. There is also significant progress toward developing the experimental tools needed for mechanical phase-space tomography or reconstruction [35,37–40]; however, all of these experiments have insufficient sensitivity to resolve features below the mechanical zero-point motion, and phase-space characterization [41] of a mechanical quantum state remains outstanding within optomechanics. One route to achieve this goal in the resolved-sideband regime is to perform single-phonon addition or subtraction for quantum-state preparation and then utilize a red-sideband drive and optical state tomography with a balanced detector, such as homodyne or heterodyne detection.

In this Letter, we describe an experimental study that observes non-Gaussian phase-space distributions generated by single-phonon and multiphonon subtraction to a thermal state of a mechanical oscillator. These operations are heralded by single-photon and multiphoton detection events following an optomechanical interaction to a laser-cooled state from room temperature. We utilize quantum-noise-limited heterodyne detection to characterize the mechanical states prepared and advance the state of the art for optics-based mechanical state tomography by more than an order of magnitude in terms of overall efficiency and added noise. We observe that the initial thermal state is transformed by these operations from a Gaussian in phase space into a ring shape with a diameter that increases with the number of phonons subtracted. Building on established results in quantum optics and recent work demonstrating that the mechanical mean occupation doubles for single-phonon addition and subtraction [36], here we additionally make the first observation that the mean occupation triples for two-phonon subtraction. This work expands the toolkit for optical control and readout of mechanical states and can be applied to experiments to exploit and characterize the non-Gaussian and nonclassical properties these operations generate.

Multiphonon subtraction scheme.—To perform n-phonon subtraction, we use a pair of optical cavity modes that are approximately spaced by the mechanical frequency to resonantly enhance the optomechanical interaction [cf. Fig. 1(a)]. Each optical mode has a linewidth much smaller than the mechanical frequency allowing operation deeply within the resolved-sideband regime. By optically driving the lower-frequency mode of the pair, the anti-Stokes scattering process is selected and a signal field in the higher-frequency cavity mode is generated. This scattering process is described by a light-mechanics beam splitter interaction with Hamiltonian $H/\hbar = G(a^\dagger b + ab^\dagger)$, where G is the linearized optomechanical coupling rate, a is the field operator of the optical signal, and b is the mechanical annihilation operator. Then, detecting n photons heralds an n-phonon subtraction to the mechanical state. For an initial mechanical thermal state $\rho_{\bar{n}}$, with mean occupation $\bar{n}$, the mechanical state following this operation may be written $\rho_{n-} \propto b^n \rho_{\bar{n}} b^{\dagger n}$. Similarly, by optically driving the upper-frequency mode, the Stokes scattering process is selected ($H/\hbar = G(ab + a^\dagger b^\dagger)$) and detecting n photons in the frequency down-shifted Stokes signal heralds n-phonon addition, $\rho_{n+} \propto b^{\dagger n} \rho_{\bar{n}} b^n$. These operations are a multiphonon generalization to Ref. [42].

When performing single-phonon or multiphonon subtraction or addition to a large thermal state, one may expect little change to the mechanical state. However, these operations significantly change the mean occupation and give rise to highly non-Gaussian distributions in mechanical phase space. Indeed, when applying an n-fold subtraction operation, the mean occupation transforms via
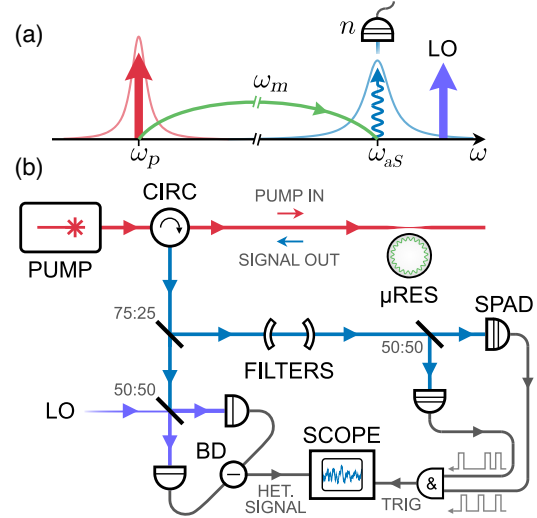

FIG. 1. Multiphonon subtraction and tomography scheme and experimental schematic. (a) Optical pumping and heralding scheme. A pair of optical resonances spaced by the mechanical angular frequency ω_m is used to resonantly enhance the optomechanical interaction. A pump field drives a mode at ω_p creating an anti-Stokes signal at ω_{aS}. An n-photon detection scheme is then used to herald n-phonon subtraction to the mechanical motion. (b) Experimental schematic. A tunable pump laser (1550 nm) drives an optical microresonator (μRES) and the backscattered anti-Stokes signal is separated from the pump with an optical circulator (CIRC). The signal is subsequently split and detected via single-photon avalanche detectors (SPADs) to herald a single- or two-phonon subtraction operation. To characterize the mechanical state prepared, heterodyne detection is performed (BD, balanced detector; LO, local oscillator), and the signal recorded on an oscilloscope triggered by SPAD detection events. The two-phonon subtraction case is shown here that uses a two-photon-coincidence measurement.

$\bar{n} \to (n+1)\bar{n}$, and for n-fold addition $\bar{n} \to (n+1)\bar{n} + n$. For $\bar{n} \gg 1$, it is noted that the mean occupation *doubles* for single-quanta addition or subtraction—which has been experimentally observed for thermal optical fields [21] and very recently for a mechanical thermal state [36]—and the mean occupation *triples* for two-quanta addition or subtraction. This significant change to the mean occupation and the non-Gaussian ring shape observed in phase space can be understood via a combination of the shift to the probability distribution of the number operator and the Bayesian inference of the nonunitary quantum-measurement process [43]. It is also important to note that in the limit $\bar{n} \gg \sqrt{n}$, the mechanical state generated by n-phonon addition is approximately the same as that generated by n-phonon subtraction. Thus, for this work, we focus on n-phonon subtraction and mechanical state readout using the anti-Stokes interaction, as this interaction is well suited for mechanical state readout and the optical field is a high-fidelity proxy for the mechanical state in the limit of high efficiency. See the Supplemental Material [44] for more mathematical details.

Experimental setup.—In this work, n-phonon subtraction is implemented by driving anti-Stokes Brillouin scattering in a BaF_2 optical microresonator. BaF_2 is an attractive material for these studies as the low optical and acoustic losses enable significant enhancement of Brillouin opto-mechanical interaction [44,45]. Here, we use a pair of optical resonances (amplitude decay rates $\kappa_p/2\pi = 7.1$ MHz, $\kappa_{aS}/2\pi = 46.9$ MHz) with a separation approximately equal to the mechanical frequency, $\omega_m/2\pi = 8.16$ GHz. The mechanical amplitude decay rate and intrinsic opto-mechanical coupling rate are $\gamma/2\pi = 3.26(39)$ MHz and $g_0/2\pi = 296(39)$ Hz, respectively [44]. The experiment was performed at 300 K, corresponding to a mean mechanical thermal occupation of $\bar{n}_{th} \simeq 766$, which, via the optomechanical coupling, was sideband cooled to $\bar{n} \simeq 453(52)$. An input pump power of $\sim$9 mW was used, corresponding to an intracavity photon number of $N_{cav} \simeq 1.2 \times 10^9$ and optomechanical coupling rate of $G/2\pi \simeq 10$ MHz, such that the system is well within the weak coupling regime ($2G < \kappa_{aS} + \gamma$). The backscattered anti-Stokes signal is coupled out of the cavity by a silica tapered fiber, with efficiency $\eta_c \simeq 0.25$, and is then separated from the forward-propagating pump field using an optical circulator before being split into two arms using a 75:25 beam splitter [cf. Fig. 1(b)]. Thus, the anti-Stokes field serves a dual role where one arm is used for heralded mechanical state preparation via photon counting and the other arm is used for mechanical state tomography via heterodyne detection.

In the 25% arm, single- and two-phonon subtraction events are heralded using two single-photon avalanche detectors (SPADs). Prior to the detectors, two fiber-based Fabry-Perot filters are used in series to filter out deleterious photons from the pump field. As the single-photon count rate [280(40) s^{-1}] is much greater than the dark count rate ($\sim$1 s^{-1}), the phonon subtraction events are heralded with high fidelity. Note that as the gate window of 3.5 ns is much less than the decay time $1/(\gamma + G^2/\kappa_{aS}) \simeq 31$ ns, the heralding of two-photon events is well approximated as simultaneous detections. See Ref. [44] for further details regarding these heralding rates. Also, note that any photons that are not detected here do not result in phonon subtraction but rather contribute to mechanical laser cooling.

In the 75% arm, balanced heterodyne detection is used to perform phase-space tomography of the mechanical states generated. The detection scheme is implemented by interfering the anti-Stokes signal and a strong local oscillator, that is frequency detuned by $\omega_{het}/2\pi = 214$ MHz with respect to the signal, onto a 50:50 beam splitter and measuring the output using a balanced photodetector. The two types of photon counting events—singles and two-photon coincidences—then trigger a high-bandwidth oscilloscope to record a time trace of the output from the balanced detector. In order to acquire sufficient statistics for the phase-space distributions and temporal dynamics of the

mechanical states for the initial, single-phonon subtracted, and two-phonon subtracted thermal states, 2.4×10^5 time traces were recorded for each case.

Mechanical state readout.—One promising route to perform mechanical quantum state characterization is to use optical homodyne or heterodyne tomography, as utilized in quantum optics, after having performed an efficient transfer of the mechanical state to the optical field. In the absence of losses or inefficiencies, if optical homodyne tomography is performed after the state transfer, then the marginals obtained allow the mechanical Wigner function to be reconstructed. And if a heterodyne measurement is performed, owing to the vacuum noise introduced with the simultaneous measurement of the two conjugate optical quadratures, the Husimi-Q function is obtained.

In practice, one of the most important aspects to such a measurement is the overall efficiency, as any loss and inefficiency reduces the quality of the phase-space distribution obtained. More specifically, optical losses result in the state of interest being convolved in phase space with vacuum noise, thus degrading the signal and even eliminating any nonclassical features if the efficiency is poor.

A versatile way to mathematically quantify the performance of a tomography experiment is to use the s-parametrized Wigner function $W_s(X_m, P_m)$ [46], as it captures the unwanted effects of noise and inefficiency in a single parameter. For our experiment here, which is limited by efficiency rather than any additional noise, the s-parameter is defined as $s = (\eta - 2)/\eta$, where η is the overall measurement efficiency of the mechanical state including the mechanics-light transduction efficiency. From the expression for s, we can see that for $\eta = 1$ we have $s = -1$, which corresponds to the Q function, and for $\eta < 1$ we have $s < -1$ corresponding to a distribution that is smoother than the Q function. Experimentally determining W_s for mechanical states fully characterizes the state allowing any statistic or measurement probability to be determined, and will aid in mechanical quantum-state engineering applications. For n-phonon subtraction, the s-parametrized Wigner function can be written as a two-dimensional convolution between the P function of the subtracted state and a Gaussian, $W_s(X_m, P_m) = (P_{n-} * G_s)(X_m, P_m)$, where $P_{n-} = (2^{-n}\bar{n}^{-n-1}/\pi n!)(X_m^2 + P_m^2)^n e^{-(X_m^2 + P_m^2)/2\bar{n}}$ and $G_s = e^{-(X_m^2 + P_m^2)/(1-s)}/\pi(1-s)$ [44].

In this experiment, via the anti-Stokes light-mechanics beam splitter interaction, the scattered optical signal acts as a proxy for the acoustic mode and is used to characterize the mechanical state generated at the time of the herald event. From the time-domain heterodyne signal we extract the two orthogonal quadrature components by demodulating the signal at the heterodyne frequency in postprocessing for each herald event. The quadrature signals are then used for two types of analysis. Firstly, we compute the variance of the ensemble of measurements for each time
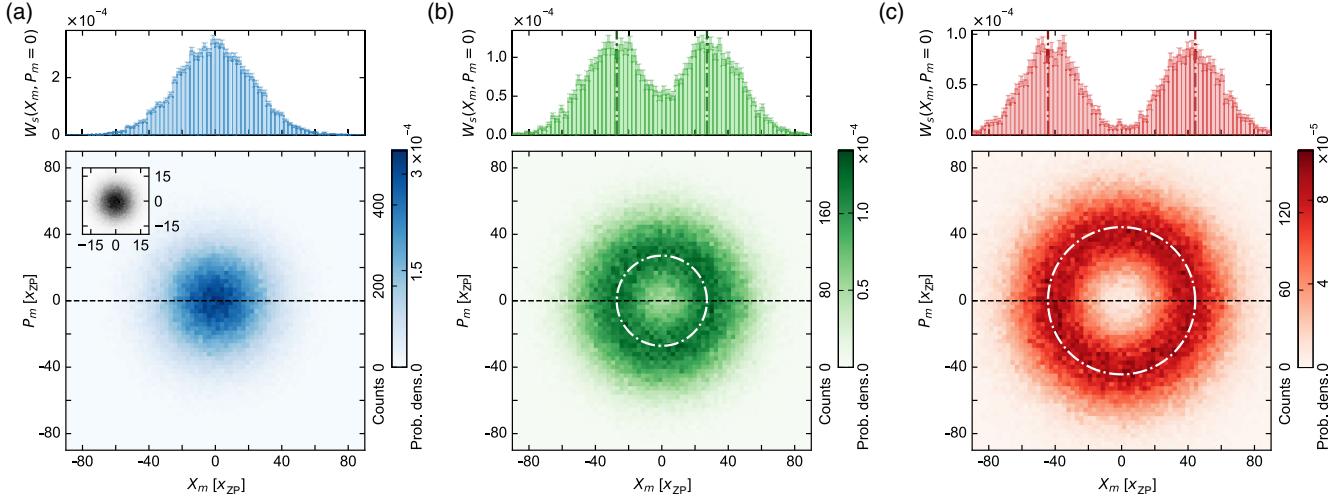
FIG. 2. Experimental s-parametrized Wigner functions W_s (bottom row), with slices through $P_m = 0$ (top row), for an (a) initial, (b) single-phonon subtracted, and (c) two-phonon subtracted mechanical thermal state. The phase-space distributions are plotted in units of the mechanical zero-point fluctuations x_{ZP} and are obtained through heterodyne detection of the optical anti-Stokes signal. The generation of non-Gaussianity from the originally Gaussian phase-space distribution is observed for single-phonon subtraction, which further grows upon two-phonon subtraction. The dash-dotted lines indicate the theoretically predicted maxima for the W_s functions. The phase-space distribution of the optical vacuum contribution is shown in the inset in (a).

about the herald event, and secondly, a two-dimensional histogram of the mechanical phase-space distribution W_s at the heralding time is obtained.

Results and discussion.—It is first instructive to discuss the overall efficiency of the mechanical state tomography η. Since we are performing a heterodyne measurement, the variance of the signal, in the steady state, away from a heralding event is $\sigma^2 = \eta \bar{n}_{\mathrm{th}} + 1$. For this experiment, we determine an overall efficiency $\eta = 0.91\%$ via independent measurement of the optical vacuum and knowledge of $\bar{n}_{\mathrm{th}}$. This efficiency yields an s parameter of $s = -219$,

corresponding to a 15 times improvement to the forefront of optics-based mechanical tomography, Ref. [38], which utilized fast pulsed measurements outside the resolved-sideband regime. Knowing η also allows one to work with units of the mechanical zero-point fluctuations x_{ZP}, rather than units of the optical vacuum, by scaling the heterodyne signals accordingly. Using this efficiency, the experimentally determined mechanical phase-space distributions W_s are plotted in Fig. 2 for the initial thermal state, the single-phonon subtracted state, and the two-phonon subtracted state. Note the highly non-Gaussian ring shape has an
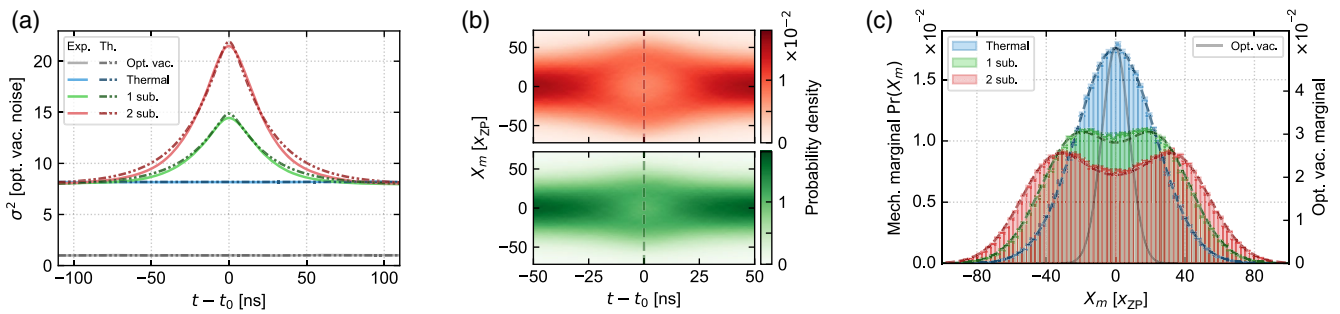

FIG. 3. Dynamics and non-Gaussian distributions of the heralded mechanical states. (a) Time evolution of the heterodyne variance in units of optical vacuum noise about the heralding event for single- and two-phonon subtracted thermal states, plotted in green and red, respectively. The optical vacuum is plotted in gray and the variance of the initial thermal state is plotted in blue. Experimentally obtained variances are shown as solid lines, and the predictions of our theoretical model are shown as dott-dashed lines. The Poissonian experimental relative uncertainty is of order 10^{-3} and is not visible on this scale. The discrepancy between theory and experiment is attributed to filtering in postprocessing and dark counts from the SPADs. At the time of the heralding event, the ratio of the heterodyne variance to the optical vacuum noise increases by a factor of 1.94 and 2.94 relative to the initial thermal state for single- and two-phonon subtraction, respectively. (b) Marginal distributions for the X_m quadrature of the mechanical oscillator as a function of time. (c) Mechanical quadrature probability distributions at the time of the heralding event, $t = t_0$, for the initial (blue), single-phonon subtracted (green), and two-phonon subtracted (red) thermal mechanical states.

increasing radius from one- to two-phonon subtraction. Theoretical predictions computed in this work for the radii of the phase-space rings [44] are indicated by the dash-dotted lines in Fig. 2.

Figure 3(a) shows the heterodyne signal variance σ^2, normalized in units of the optical vacuum noise, as a function of time about the herald event. For the single- and two-phonon subtraction cases, it is observed that the variance increases at the time of the herald event by a factor of 1.94 and 2.94, respectively, compared to the mean variance of 7.96. This is in close agreement with the variance "doubling" and "tripling" from the theoretical predictions [44] shown, for which only the heralding time t_0 is a free fitting parameter. We attribute the small difference between our experimental observations and the theoretical prediction to be due to the filtering in the quadrature demodulation, the small level of dark counts in the SPAD detectors, and the optical filtering performed in the heralding arm. From this variance, it is seen that the contribution from optical vacuum is 14%, or equivalently, the overall measurement efficiency yielded a total added noise of $|s|/2 = 110$ mechanical quanta.

In Fig. 3(b), we have plotted the marginals $\Pr(X_m) = \int dP_m W_s(X_m, P_m)$ as a function of time about the herald event. This plot illustrates how the state transforms by the single- and two-phonon subtraction operations from an initial Gaussian state to a non-Gaussian state that has a bimodal quadrature probability distribution and then returns to thermal equilibrium. In Fig. 3(c), the mechanical quadrature probability distributions $\Pr(X_m)$ at the time of the herald event are plotted. At this time, the non-Gaussianity generated is most significant and the initial distribution can be compared with the bimodal distributions generated via single- and two-phonon subtraction together with the theoretical prediction [44] overlaid.

Conclusions and outlook.—Utilizing both photon counting and optical heterodyne measurements, we report the first experimental generation and phase-space tomography of non-Gaussian states of mechanical motion via single- and two-phonon subtraction to a laser-cooled thermal state. In achieving this milestone this work advances optics-based mechanical tomography by more than an order of magnitude in the s parameter. These advancements make key steps toward mechanical phase-space tomography of nonclassical mechanical states, which remains outstanding within optomechanics. Furthermore, the techniques developed here can be utilized for a wide range of mechanical quantum-state engineering applications taking advantage of single- and multiphonon addition and subtraction operations. In particular, these operations can be applied to a mechanical squeezed state for superposition state preparation [47], and reservoir engineering has been discussed as a promising route to generate the squeezing in such protocols [48,49].

For this experiment, we would like to highlight four key pathways for improvement: (i) operation at cryogenic temperature to reduce the material contributions to the mechanical decay rate [1–3,50], (ii) increasing the drive strength and utilizing the optomechanical strong coupling available in Brillouin optomechanical systems [51], (iii) further tapered fiber and microresonator optimization to enable better optical coupling with respect to the intrinsic cavity losses, and (iv) utilizing a Stokes interaction for mechanical state preparation, followed by an anti-Stokes interaction for the readout, to provide a route to make the readout more independent and remove the beam splitter for the single-photon detection to improve the efficiency. Implementing these four improvements provides a promising path to achieving an overall anti-Stokes readout measurement efficiency exceeding 50%. Achieving this efficiency, together with performing quantum-noise-limited homodyne detection, yields an s parameter of $s > -1$, which is required to observe negativity of a quantum phase-space distribution—a key signature of nonclassicality and a powerful resource for quantum-enhanced technologies. Additionally, achieving a higher-efficiency anti-Stokes interaction with the paths above provides a means to implement a quantum memory device that can efficiently write and read quantum states to and from the acoustic mode.

Note added.—Recently, we became aware of related experimental work also observing mechanical non-Gaussianity [52].

---

[1] S. Galliou, M. Goryachev, R. Bourquin, P. Abbe, J. P. Aubry, and M. E. Tobar, Sci. Rep. **3**, 2132 (2013).

[2] W. H. Renninger, P. Kharel, R. O. Behunin, and P. T. Rakich, Nat. Phys. **14**, 601 (2018).

[3] G. S. MacCabe, H. Ren, J. Luo, J. D. Cohen, H. Zhou, A. Sipahigil, M. Mirhosseini, and O. Painter, Science **370**, 840 (2020).

[4] A. P. Higginbotham, P. S. Burns, M. D. Urmey, R. W. Peterson, N. S. Kampel, B. M. Brubaker, G. Smith, K. W. Lehnert, and C. A. Regal, Nat. Phys. **14**, 1038 (2018).

[5] M. Mirhosseini, A. Sipahigil, M. Kalaee, and O. Painter, Nature (London) **588,** 599 (2020).

[6] P. H. Kim, B. D. Hauer, C. Doolin, F. Souris, and J. P. Davis, Nat. Commun. **7,** 13165 (2016).

[7] F. Monteiro, S. Ghosh, A. G. Fine, and D. C. Moore, Phys. Rev. A **96,** 063841 (2017).

[8] D. Carney, A. Hook, Z. Liu, J. M. Taylor, and Y. Zhao, New J. Phys. **23,** 023041 (2021).

[9] S. Bose, K. Jacobs, and P. L. Knight, Phys. Rev. A **59,** 3204 (1999).

[10] W. Marshall, C. Simon, R. Penrose, and D. Bouwmeester, Phys. Rev. Lett. **91,** 130401 (2003).

[11] A. Bassi, K. Lochan, S. Satin, T. P. Singh, and H. Ulbricht, Rev. Mod. Phys. **85,** 471 (2013).

[12] I. Pikovski, M. R. Vanner, M. Aspelmeyer, M. S. Kim, and Č. Brukner, Nat. Phys. **8,** 393 (2012).

[13] S. Bose, A. Mazumdar, G. W. Morley, H. Ulbricht, M. Toros, M. Paternostro, A. A. Geraci, P. F. Barker, M. S. Kim, and G. Milburn, Phys. Rev. Lett. **119,** 240401 (2017).

[14] C. Marletto and V. Vedral, Phys. Rev. Lett. **119,** 240402 (2017).

[15] D. Leibfried, D. M. Meekhof, B. E. King, C. Monroe, W. M. Itano, and D. J. Wineland, Phys. Rev. Lett. **77,** 4281 (1996).

[16] C. Flühmann, T. L. Nguyen, M. Marinelli, V. Negnevitsky, K. Mehta, and J. P. Home, Nature (London) **566,** 513 (2019).

[17] A. I. Lvovsky, H. Hansen, T. Aichele, O. Benson, J. Mlynek, and S. Schiller, Phys. Rev. Lett. **87,** 050402 (2001).

[18] A. Ourjoumtsev, R. Tualle-Brouri, J. Laurat, and P. Grangier, Science **312,** 83 (2006).

[19] J. S. Neergaard-Nielsen, B. M. Nielsen, C. Hettich, K. Molmer, and E. S. Polzik, Phys. Rev. Lett. **97,** 083604 (2006).

[20] T. Gerrits, S. Glancy, T. S. Clement, B. Calkins, A. E. Lita, A. J. Miller, A. L. Migdall, S. W. Nam, R. P. Mirin, and E. Knill, Phys. Rev. A **82,** 031802(R) (2010).

[21] A. Zavatta, V. Parigi, and M. Bellini, Phys. Rev. A **75,** 052106 (2007).

[22] V. Parigi, A. Zavatta, M. S. Kim, and M. Bellini, Science **317,** 1890 (2007).

[23] Yu. I. Bogdanov, K. G. Katamadze, G. V. Avosopiants, L. V. Belinsky, N. A. Bogdanova, A. A. Kalinkin, and S. P. Kulik, Phys. Rev. A **96,** 063803 (2017).

[24] S. Deleglise, I. Dotsenko, C. Sayrin, J. Bernu, M. Brune, J.-M. Raimond, and S. Haroche, Nature (London) **455,** 510 (2008).

[25] R. McConnell, H. Zhang, J. Hu, S. Cuk, and V. Vuletic, Nature (London) **519,** 439 (2015).

[26] M. Hofheinz *et al.*, Nature (London) **459,** 546 (2009).

[27] Y. Chu, P. Kharel, T. Yoon, L. Frunzio, P. T. Rakich, and R. J. Schoelkopf, Nature (London) **563,** 666 (2018).

[28] K. J. Satzinger *et al.*, Nature (London) **563,** 661 (2018).

[29] K. C. Lee, B. J. Sussman, M. R. Sprague, P. Michelberger, K. F. Reim, J. Nunn, N. K. Langford, P. J. Bustard, D. Jaksch, and I. A. Walmsley, Nat. Photonics **6,** 41 (2012).

[30] K. A. G. Fisher, D. G. England, Jean-Philippe W. MacLean, P. J. Bustard, K. Heshami, K. J. Resch, and B. J. Sussman, Phys. Rev. A **96,** 012324 (2017).

[31] S. T. Velez, K. Seibold, N. Kipfer, M. D. Anderson, V. Sudhir, and C. Galland, Phys. Rev. X **9,** 041007 (2019).

[32] R. Riedinger, S. Hong, R. A. Norte, J. A. Slater, J. Shang, A. G. Krause, V. Anant, M. Aspelmeyer, and S. Gröblacher, Nature (London) **530,** 313 (2016).

[33] J. D. Cohen, S. M. Meenehan, G. S. MacCabe, S. Gröblacher, A. H. Safavi-Naeini, F. Marsili, M. D. Shaw, and O. Painter, Nature (London) **520,** 522 (2015).

[34] I. Galinskiy, Y. Tsaturyan, M. Parniak, and E. S. Polzik, Optica **7,** 718 (2020).

[35] M. Ringbauer, T. J. Weinhold, L. A. Howard, A. G. White, and M. R. Vanner, New J. Phys. **20,** 053042 (2018).

[36] G. Enzian, J. J. Price, L. Freisem, J. Nunn, J. Janousek, B. C. Buchler, P. K. Lam, and M. R. Vanner, Phys. Rev. Lett. **126,** 033601 (2021).

[37] M. R. Vanner, J. Hofer, G. D. Cole, and M. Aspelmeyer, Nat. Commun. **4,** 2295 (2013).

[38] J. T. Muhonen, G. R. La Gala, R. Leijssen, and E. Verhagen, Phys. Rev. Lett. **123,** 113601 (2019).

[39] O. Suchoi, K. Shlomi, L. Ella, and E. Buks, Phys. Rev. A **91,** 043829 (2015).

[40] M. Rashid, M. Toros, and H. Ulbricht, Quantum Meas. Quantum Metrol. **4,** 17 (2017).

[41] M. R. Vanner, I. Pikovski, and M. S. Kim, Ann. Phys. (Berlin) **527,** 15 (2015).

[42] M. R. Vanner, M. Aspelmeyer, and M. S. Kim, Phys. Rev. Lett. **110,** 010504 (2013).

[43] S. M. Barnett, G. Ferenczi, C. R. Gilson, and F. C. Speirits, Phys. Rev. A **98,** 013809 (2018).

[44] See Supplemental Material at http://link.aps.org/supplemental/10.1103/PhysRevLett.127.243601 for further details on the experimental setup, theoretical model, and system characterization.

[45] G. Lin, S. Diallo, K. Saleh, R. Martineghi, J. C. Beugnot, T. Sylvestre, and Y. K. Chembo, Appl. Phys. Lett. **105,** 231103 (2014).

[46] U. Leonhardt and H. Paul, Phys. Rev. A **48,** 4598 (1993); U. Leonhardt, *Measuring the Quantum State of Light* (Cambridge University Press, Cambridge, England, 1997).

[47] T. J. Milburn, M. S. Kim, and M. R. Vanner, Phys. Rev. A **93,** 053818 (2016).

[48] I. Shomroni, L. Qiu, and T. J. Kippenberg, Phys. Rev. A **101,** 033812 (2020).

[49] H. Zhan, G. Li, and H. Tan, Phys. Rev. A **101,** 063834 (2020).

[50] S. Ohno, T. Sonehara, E. Tatsu, A. Koreeda, and S. Saikan, Rev. Sci. Instrum. **77,** 123104 (2006).

[51] G. Enzian, M. Szczykulska, J. Silver, L. Del Bino, S. Zhang, I. A. Walmsley, P. Del'Haye, and M. R. Vanner, Optica **6,** 7 (2019).

[52] R. N. Patel, T. P. McKenna, Z. Wang, J. D. Witmer, W. Jiang, R. Van Laer, C. J. Sarabalis, and A. H. Safavi-Naeini, Phys. Rev. Lett. **127,** 133602 (2021).